Syntheses and characterization of the cubic uranium chalcogenides Rh2U6S15, Cs2Ti2U6Se15, Cs2Cr2U6Se15 and Cs2Ti2U6Te15

Matthew Ward, George Oh, Adel Mesbah, Minseong Lee, Eun Sang Choi, James Ibers

Syntheses and characterization of the cubic uranium chalcogenides $Rh_2U_6S_{15}$, $Cs_2Ti_2U_6Se_{15}$, $Cs_2Cr_2U_6Se_{15}$, and $Cs_2Ti_2U_6Te_{15}$

Matthew D. Ward[a], George N. Oh[a], Adel Mesbah[a,b], Minseong Lee[c], Eun Sang Choi[c], and James A. Ibers[a,*]

[a]*Department of Chemistry, Northwestern University, Evanston, IL 60208-3113, USA*

[b]*ICSM, UMR 5257 CEA / CNRS / UM2 / ENSCM, Site de Marcoule - Bât. 426, BP 17171, 30207 Bagnols-sur-Cèze cedex, France*

[c]*Department of Physics and National High Magnetic Field Laboratory, Florida State University, Tallahassee, Florida, 32310-3706, United States*

Keywords: uranium chalcogenides; syntheses; structures; magnetism

Abstract

The compounds $Rh_2U_6S_{15}$, $Cs_2Ti_2U_6Se_{15}$, $Cs_2Cr_2U_6Se_{15}$, and $Cs_2Ti_2U_6Te_{15}$ have been synthesized at 1173 K. All crystallize in space group O_h^9–$Im\bar{3}m$ of the cubic system. $Rh_2U_6S_{15}$ has a framework structure with three-dimensional channels. The compounds $Cs_2Ti_2U_6Se_{15}$, $Cs_2Cr_2U_6Se_{15}$, and $Cs_2Ti_2U_6Te_{15}$ have structures similar to that of $Rh_2U_6S_{15}$, but with Cs cations variably filling the channels. In all four structures the transition element is octahedrally coordinated by chalcogens and the uranium atom is in a bicapped trigonal-prismatic arrangement. The temperature dependence of the magnetic susceptibility of $Cs_2Cr_2U_6Se_{15}$ implies both Cr and U magnetic contributions. From these data the compound is not antiferromagnetic, but it could have either a ferrimagnetic or a ferromagnetic ground state.

1. Introduction

Ternary and quaternary uranium chalcogenide compounds containing d-metals have been the subject of extensive research [1-4]. There is considerable interest in compounds that contain d-metals, as interactions between the localized 5*f* electrons and d electrons can lead to interesting physical properties [5-9]. Many of these compounds such as MU_8Q_{17} [10-18] and MUQ_3

*Corresponding author. Fax: +1 847 491 2976

E-mail address: ibers@chem.northwestern.edu (J.A.Ibers)

[3,12,19-21] contain 3d metals, whereas fewer compounds have been characterized that contain 4d metals. Examples of these include: AAgUQ_3 (A = Rb, Cs, Q = S, Se) [22], A_2Pd$_3$UQ_6 [23], $Rh_2U_6Se_{15.555}$ [24], $CsZrUTe_5$ [25], MUQ_3 (M = Ru, Rh, Pd, Q = S, Se) [26,27], $A_2Pd_4U_6Q_{17}$ (A = Rb, Cs, Q = S, Se) [28], Mo_6UQ_8 (Q = S, Se) [29], Ba_3AgUS_6 [30], and $Ba_9Ag_{10}U_4S_{24}$ [31]. Because 3d, 4d, and 5d metals differ in size and in preferred coordination environments, it is unlikely that the structure of a given U/3d/Q compound will be same as those of the corresponding U/4d/Q or U/5d/Q compounds. Nevertheless, such structures may be related. Here we present the synthesis and characterization of three new 3d-containing quaternary uranium chalcogenides, namely $Cs_2Ti_2U_6Se_{15}$, $Cs_2Cr_2U_6Se_{15}$, and $Cs_2Ti_2U_6Te_{15}$, whose structures are closely related to that of $Rh_2U_6S_{15}$ also reported here and to that of the previously reported 4d- and 5d-containing $M_2U_6Q_{15.555}$ (M = Rh, Ir, Q = S, Se) compounds [24]. The magnetic properties of $Cs_2Cr_2U_6Se_{15}$ turn out to be especially interesting.

2. Experimental

2.1 Syntheses

The following reactants were used as received: Ti (Alfa 99.5%), Cr (Aesar 99.99%), Rh (Johnson-Mathey 99.95%), S (Mallinckrodt 99.6%), Se (Cerac 99.999%), Te (Aldrich 99.8%), and CsCl (MP Biomedicals 99.9%). U powder was obtained through the hydridization of depleted-U turnings (Mfg Sci. Corp.) followed by decomposition of the hydride under vacuum [32]. US_2 powder was obtained by the stoichiometric reaction of the elements at 1223 K. The reactants were loaded into carbon-coated fused-silica tubes in an Ar-filled glove box, evacuated to 10^{-4} Torr, and flame sealed. Each tube was heated from 298 K to 1173 K in 12 h, held there for 6 h, cooled to 1073 K over 12 h, and held there for 96 h. The tube was then cooled to 773 K over 60 h and finally to 298 K in a further 12 h. Semi-quantitative elemental analysis of the products was carried out with the use of a Hitachi S-3400 SEM equipped for EDX analysis.

Synthesized crystals were stable in air for several months, as judged from unit-cell determinations. However, surface oxidation of the crystals with formation of UOQ (Q = S, Se, Te) compounds cannot be excluded.

Synthesis of $Rh_2U_6S_{15}$. Black prisms of $Rh_2U_6S_{15}$ were obtained by combining US_2, Rh, and S in a CsCl flux. The reaction contained 0.0381g (0.126 mmol) US_2, 0.0129g (0.125 mmol) Rh, 0.0121g (0.377mmol) S, and 0.0750g (0.4455 mmol) CsCl. Analysis: Rh:U:S≈2:6:15. The yield of $Rh_2U_6S_{15}$ was about 75 wt% based on U. The reaction also yielded U/S binaries and excess flux.

Synthesis of $Cs_2Ti_2U_6Se_{15}$. Black blocks of $Cs_2Ti_2U_6Se_{15}$ were first found unexpectedly from the reaction of 0.0300 g (0.126 mmol) U, 0.0169 g (0.214 mmol) Se, 0.0065 g (0.013 mmol) Cs_2Se_3, and 0.0123 g (0.101 mmol) Sb. The reaction was heated to 1273 K in 48 h, held there for 4 h, cooled to 1223 K in 12 h, and held there for 192 h. The reaction was then cooled to 873 K in 96 h and then to 298 K in a further 96 h. The reaction afforded black rectangular blocks and columns that were washed with water to remove excess flux. Elemental analysis revealed the presence of Cs, U, Se, and, surprisingly, Ti. It was subsequently determined that the U used to produce U powder was contaminated with about 10 wt% Ti. According to the manufacturer, the U turnings were produced using a blade made with an Al/Ti alloy and owing to the hardness of U some of the blade was stripped during the turning process.

These crystals have been labeled as $Cs_2Ti_2U_6Se_{15}$-1. A rational synthesis of $Cs_2Ti_2U_6Se_{15}$ was achieved by the reaction of 0.0300g (0.126 mmol) U, 0.0060g (0.126 mmol) Ti, 0.0298g (0.378 mmol) Se, and 0.0500g (0.2970 mmol) CsCl heated under the profile listed for Syntheses. Analysis: Cs:Ti:U:Se≈2:2:6:15. These crystals have been labeled as $Cs_2Ti_2U_6Se_{15}$-2. The reaction for $Cs_2Ti_2U_6Se_{15}$-2 yielded black prisms of $Cs_2Ti_2U_6Se_{15}$ in about 90 wt% based on U as well as a few crystals of TiU_8Se_{17} and excess flux.

Synthesis of $Cs_2Cr_2U_6Se_{15}$. Black prisms of $Cs_2Cr_2U_6Se_{15}$ were obtained by the reaction of the elements in a CsCl flux. The reaction contained 0.0300g (0.126 mmol) U, 0.0065g (0.125 mmol) Cr, 0.0298g (0.378mmol) Se, and 0.0500g (0.2970 mmol) CsCl. Analysis:Cs:Cr:U:Se≈2:2:6:15. The reaction for $Cs_2Cr_2U_6Se_{15}$ yielded black prisms of $Cs_2Cr_2U_6Se_{15}$ in about 90 wt% based on U as well as a few crystals of CrU_8Se_{17} and excess flux. Several crystals of $Cs_2Cr_2U_6Se_{15}$ were washed with water and dried with acetone to remove excess flux and then ground into a fine powder. The X-ray powder diffration pattern confirmed the removal of the excess of flux and CrU_8Se_{17} was not detected.

Synthesis of $Cs_2Ti_2U_6Te_{15}$. In an effort to reproduce the compound $CsTiU_3Te_9$ [33], black blocks of $Cs_2Ti_2U_6Te_{15}$ were found from the reaction of U 0.0300 g (0.126 mmol), 0.0060 g (0.126 mmol) Ti, 0.0482 g (0.378 mmol) Te, and 0.1000 g (0.594 mmol) CsCl when heated under the profile above. The reaction afforded black rectangular plates of $CsTiU_3Te_9$ and black blocks of $Cs_2Ti_2U_6Te_{15}$ along with excess flux. Elemental analysis revealed the presence of Cs, Ti, U, and Te in both compounds. Although a number of reactions over a period of several months afforded $CsTiU_3Te_9$, only one also yielded $Cs_2Ti_2U_6Te_{15}$ as an additional product. This reaction produced black plates of $CsTiU_3Te_9$ and black blocks of $Cs_2Ti_2U_6Te_{15}$ in about 50 and 10 wt%, respectively, based on U. U/Te binaries and excess flux were also detected.

2.2 Structure Determinations

Single-crystal X-ray diffraction data were collected at 100(2) K on an APEX2 X-ray diffractometer equipped with graphite-monochromatized Mo$K\alpha$ radiation [34]. The crystal-to-detector distance was 60 mm; the exposure time was 10 sec/frame. Collection of intensity data, cell refinement, and data reduction were performed using APEX2 as a series of 0.3□ scans in φ and ω [34]. Face-indexed absorption, incident beam, and decay corrections were performed by the program SADABS [35]. All structures were solved using the SHELX14 suite of programs [36]. Atom positions were standardized using the program STRUCTURE TIDY [37]. Structure drawings were made using the program CRYSTALMAKER [38]. Further details are given in Tables 1, 2, and 3 and in the Supporting Information.

Although the solution and refinement of the framework channel structure, $Rh_2U_6S_{15}$, were straightforward, the refinements of the $Cs_2Ti_2U_6Se_{15}$, $Cs_2Cr_2U_6Se_{15}$, and $Cs_2Ti_2U_6Te_{15}$ structures were complicated because of the filling of the channels by Cs atoms centered on 0,½,½ (Cs1) and 0,0,z (Cs2). On the assumption that the formal charges are Ti^{2+}, Cr^{2+}, and U^{4+} a model was developed to achieve charge balance that involved the site occupancies of the Cs1 and Cs2 sites. The constraint equation is $8 = 6f_1 + 12f_2$, where f_1 and f_2 are the occupancies of the Cs1 and Cs2 sites, respectively. If the Cs1 site were fully occupied then f_1 would be 1.000 and f_2 would be 0.167. The results of the constrained refinements for $Cs_2Ti_2U_6Se_{15}$-1, $Cs_2Ti_2U_6Se_{15}$-2,

$Cs_2Cr_2U_6Se_{15}$, and $Cs_2Ti_2U_6Te_{15}$ were 1.003(3) and 0.165(1); 0.820(4) and 0.256(2); 0.830(4) and 0.252(2); and 0.990(4) and 0.172(2), respectively. This model is not completely satisfactory because it results in unreasonably short Cs2−Cs2 distances as well as some unreasonable Cs2 displacement parameters.

2.3 Inductively coupled plasma (ICP) Analysis

Several crystals of $Cs_2Cr_2U_6Se_{15}$ were washed with water and dried with acetone to remove excess flux and then ground into a fine powder. A 10.0 mg powder sample was then selected and sent to ALS Environmental for ICP analysis. Elemental analyses for Cr, U, and Se were completed at ALS-Tuscon and elemental analysis of Cs was completed at ALS-Salt Lake City. The analyses were not repeated so it is difficult to assign uncertainties to these results. Found (wt%): Cs,8.2; Cr, 3.67; U, 45.94; Se, 37.80. Theory: Cs, 8.9; Cr, 3.5; U, 47.9; Se, 39.7. If we assume a 95% recovery of the sample then the experimental results are 8.6 %, 3.9 %, 48.2 %, and 39.7 % in reasonable agreement with theory.

2.4 Magnetic Measurements

Magnetic susceptibility measurements were collected with the use of a Quantum Design MPMS5 SQUID magnetometer on 12.1 mg of ground single crystals of $Cs_2Cr_2U_6Se_{15}$. These were loaded into a gelatin capsule. Zero-field cooled (ZFC) and field-cooled (FC) susceptibility data were collected between 5 and 300 K at an applied field of 0.5 T. Magnetization measurements were collected at 5 K with applied fields of 0 T to 5 T.

3. Results

3.1 Syntheses and Structures

$Rh_2U_6S_{15}$. Previously, the compound $Rh_2U_6S_{15.5}$ was synthesized as a powder by the reaction of US_2, Rh, and S at 1673 K in an H_2S stream [24]. Powders of the compounds

$Ir_2U_6S_{15.5}$, $Ir_2U_6Se_{15.5}$, and $Rh_2U_6Se_{15.5}$ were obtained from the reaction of UQ_2, M, and Q at 1453 K [24]. Single crystals of $Ir_2U_6Se_{15.5}$ and $Rh_2U_6Se_{15.5}$ were obtained with the use of I_2 as a transport agent.

Presently, single crystals of $Rh_2U_6S_{15}$ were obtained from the reaction of US_2, Rh, and S in a CsCl flux at 1173 K. In agreement with earlier single-crystal X-ray diffraction studies of $Ir_2U_6Se_{15.5}$ and $Rh_2U_6Se_{15.5}$ [24] we find that $Rh_2U_6S_{15}$ crystallizes in the space group O_h^9–$Im\bar{3}m$ of the cubic system with four formula units in the unit cell. The asymmetric unit comprises the following atoms with their site symmetries: U1 (*m.m*2), Rh1 (.$\bar{3}$*m*), S1 (..*m*), and S2 ($\bar{4}$*m*.2). The structure of $Rh_2U_6S_{15}$ is a three-dimensional framework (Fig. 1). The coordination within the framework structure creates three-dimensional channels that are surrounded by the S1 and S2 atoms. In the previous study of $Ir_2U_6Se_{15.5}$ and $Rh_2U_6Se_{15.5}$ [24] a third chalcogen, (S3, 4/*mm.m*), was assigned to these channels where it was weakly bonded to 12 chalcogen atoms within the framework. We find no evidence for such an assignment in the structure of $Rh_2U_6S_{15}$. Hence, the formula $Rh_2U_6S_{15}$ is charge balanced with the assignment of formal oxidation states of +3, +4, and −2 to Rh, U, and S, respectively.

Within the framework, each Rh atom is coordinated by six S atoms in an octahedral arrangement (Fig. 2) and is surrounded by the six nearest U atoms that at a distance of 3.412(1) Å (Table 2). Each of the U atoms face-shares three S atoms on six of the eight faces of the RhS_6 octahedron. The unshared faces are opposite each other and face inwards towards two of the three-dimensional channels. The Rh−S interatomic distance of 2.382(2) Å, may be compared with those in $RhUS_3$ of 2.353(1) to 2.508(2) Å [26].

Each U atom is surrounded by eight S atoms in a bicapped trigonal-prismatic arrangement (Fig. 3). Each U atom face-shares three S atoms of the capped faces with the four nearest U atoms 3.991(1) Å away. Each of these four U atoms shares one of the capping and two of the non-capping S atoms of the bicapped trigonal prism. Four additional U atoms 5.536 (1) Å away corner-share with one of the four S atoms on the uncapped face of the trigonal prism. Each U atom also face-shares a capping S atom and two S of the uncapped face with two Rh atoms. The U−Rh distance is 3.412(1) Å. The U−S interatomic distances range from 2.754(1) to 2.856(2) Å, which can be compared with the U−S distances for bicapped trigonal prisms in $RhUS_3$ (2.687(3) to 2.950(2) Å) [26] and the MU_8S_{17} compounds (2.680(2) to 3.031(3) Å) [18].

[$Cs_2M_2U_6Q_{15}$]: $Cs_2Ti_2U_6Se_{15}$, $Cs_2Cr_2U_6Se_{15}$, and $Cs_2Ti_2U_6Te_{15}$. Single crystals of these compounds were synthesized from the reaction of U, *M*, and *Q* in a CsCl flux at 1173 K.

The structure of $Cs_2M_2U_6Q_{15}$ is analogous to that of the $Rh_2U_6S_{15}$ parent structure with a three-dimensional framework made up of *M*, U, and *Q* atoms that create three-dimensional channels. However, the substitution of M^{2+} for Rh^{3+} leads to the three-dimensional channels being variably filled by Cs1 (4/*mm.m*) and Cs2 (4*m.m*) atoms (Fig. 4).

The axial dimension (Table 1) for $Cs_2Ti_2U_6Se_{15}$-2 is significantly shorter at 13.9062(8) Å than that of 14.0029(4) Å for $Cs_2Ti_2U_6Se_{15}$-1. The Cs positions in $Cs_2Ti_2U_6Se_{15}$-1 are fully occupied whereas those in $Cs_2Ti_2U_6Se_{15}$-2 (and also $Cs_2Cr_2U_6Se_{15}$) are not. The result is expansion of the overall framework. This difference may be the result of the slower rate of cooling in the synthesis of $Cs_2Ti_2U_6Se_{15}$-1 compared with those of $Cs_2Ti_2U_6Se_{15}$-2 and $Cs_2Cr_2U_6Se_{15}$. Note that despite the same heating profile as $Cs_2Ti_2U_6Se_{15}$-2 and $Cs_2Cr_2U_6Se_{15}$, $Cs_2Ti_2U_6Te_{15}$ has fully occupied Cs positions. The increase in size from Se to Te expands the dimensions of the framework so perhaps a slower cooling rate is not required for preferential occupation of the Cs1 site.

As in $Rh_2U_6S_{15}$, each *M* atom in $Cs_2M_2U_6Q_{15}$ is coordinated by six *Q* atoms in an octahedral arrangement. This octahedron again shares three *Q* atoms on six of its eight faces with the six nearest U atoms. The *M*−U distances are 3.605(1), 3.581(1), and 3.585(1) Å for Ti-1, Ti-2 and Cr, respectively. The *M*−Se distances of 2.578(1), 2.566(1), and 2.531(1) Å for Ti-1, Ti-2, and Cr may be compared with distances in MU_8Se_{17} (*M* = Ti, Cr) of 2.427(1) to 2.569(1) Å [18]. For the $Cs_2Ti_2U_6Te_{15}$ compound the Ti1−Te1 distances of 2.787 (1) Å may be compared with those of 2.728(1) to 2.813(1) Å in $ATiU_3Te_9$ (*A* = Rb, Cs) [33].

The U atoms in $Cs_2M_2U_6Q_{15}$ are coordinated to eight *Q* atoms in a bicapped trigonal-prismatic arrangement. These UQ_8 units share their *Q* atoms with the surrounding U and M atoms as described for $Rh_2U_6S_{15}$. The U−Se distances (2.924(1) to 3.042(1) Å) are normal and may again be compared with those in MU_8Se_{17} [18]. The U−Te distances in $Cs_2Ti_2U_6Te_{15}$ range from 3.156(1) to 3.264(1) Å and may be compared with those of 2.996(3) to 3.276(3) Å in $ATiU_3Te_9$ (*A* = Rb, Cs) [33].

The Cs1 atoms in $Cs_2M_2U_6Se_{15}$ are surrounded by 12 Se atoms and have eight Cs1−Se1 interactions ranging from 3.606(1) to 3.652(1) Å and four Cs1−Se2 ranging from 3.477(1) to

3.501(1) Å. For $Cs_2Ti_2U_6Te_{15}$, the Cs1−Te1 interatomic distance is 3.883(1) Å and the Cs1−Te2 distance is 3.753(1) Å. The Cs2 atoms have four short, eight intermediate, and eight long Cs2−*Q*1 interactions. The short Cs2−Se1 interatomic distances range from 3.596(6) Å for $Cs_2Ti_2U_6Se_{15}$-1 to 3.839(10) Å for $Cs_2Cr_2U_6Se_{15}$. For $Cs_2Ti_2U_6Te_{15}$, the Cs2−Te1 distances are 3.733 (4) Å. Note that the Cs2−Te1 distances for $Cs_2Ti_2U_6Te_{15}$ are shorter than the Cs2−Se1 distances in $Cs_2Ti_2U_6Se_{15}$-2 and $Cs_2Cr_2U_6Se_{15}$. The remaining eight intermediate and eight long Cs2−*Q*1 interactions occur with *Q* atoms on the opposite side of the channel. Because the Cs2 atoms are at the vertices of an octahedron, they do not occupy the center of the channels (Fig. 5) and thus have a range of Cs2−Se1 and apparent Cs2−Cs2 interatomic distances.

3.2 Magnetic Measurements for $Cs_2Cr_2U_6Se_{15}$

Fig. 6 plots the molar susceptibility χ_m vs. T of $Cs_2Cr_2U_6Se_{15}$ for both FC and ZFC measurements. The FC and ZFC data do not differ much at higher temperatures, but they diverge near 84 K where the ZFC data show a sharp transition. Because both ferromagnets and ferrimagnets can show such a bifurcation at the transition temperature, the magnetic ground state can be either ferrimagnetic or ferromagnetic. The sharply decreasing ZFC curve below the transition temperature may indicate that coercivity is larger than 500 Oe [39].

A plot of $(\chi_m - \chi_0)^{-1}$ vs. T is presented in Fig. 7. The high-temperature region above 125 K was fit to the modified Curie-Weiss relation, $\chi_m = C/(T-\theta) + \chi_0$, where C is the Curie constant, χ_0 is the temperature-independent susceptibility, and θ is the Weiss temperature. The Curie constant is related to the effective moment (μ_{eff}) and the number of the magnetic ions per mole (N) through $C = N\,\mu_{eff}^2$. From the fitting we obtained C = 8.0(1) emu/mol· K, θ = 51(2) K, μ_{eff} = 8.0(1) μ_B, and $\chi_0 = -1.0(1) \times 10^{-3}$ emu/mol.

The possible magnetic ions in $Cs_2Cr_2U_6Se_{15}$ comprise two Cr^{2+} and six U^{4+}per formula unit, and the Curie constant is the sum of their individual contributions. Therefore, the total effective moment can be expressed $\mu_{eff} = [2\times\mu_{eff}^2(Cr^{2+}) + 6\times\mu_{eff}^2(U^{4+})]^{1/2}$, where μ_{eff} (Cr^{2+}) and μ_{eff} (U^{4+}) are the effective magnetic moments of Cr^{2+} and U^{4+}, respectively. The spin-only free ion effective moment of Cr^{2+} is either 2.8 μ_B or 4.9 μ_B depending on the spin state (low-spin or high-spin) and that of U^{4+} is about 3.6 μ_B with *L*-*S* coupling. Then, the total effective moment of

$Cs_2Cr_2U_6Se_{15}$ can range from 4.0 (low-spin Cr^{2+}, non-magnetic U^{4+}), 6.9 (high-spin Cr^{2+}, non-magnetic U^{4+}), 8.8 (non-magnetic Cr^{2+}, magnetic U^{4+}), 9.7 (low-spin Cr^{2+}, magnetic U^{4+}) to 11.2 μ_B (high-spin Cr^{2+}, magnetic U^{4+}).

It is clear that the U^{4+} center is magnetic because the observed value of μ_{eff} (8.0 μ_B) is larger than any hypothetical value with non-magnetic U^{4+}. The scenario that gives a value of μ_{eff} closest to the observed one is that of non-magnetic Cr^{2+}. But note that the effective moments of uranium compounds are usually smaller than the free-ion value because of the crystalline electric field (CEF) effect or itinerant magnetism. Also, it is unlikely that Cr^{2+} is completely non-magnetic. Therefore, it is more reasonable to assume both Cr^{2+} and U^{4+} possess magnetic moments. Then the effective moment of U can be between 1.6 μ_B (high-spin Cr^{2+}) and 2.8 μ_B (low-spin Cr^{2+}). Because S^{2-} is a weak-field ligand we would expect Se^{2-} also to be and hence Cr^{2+} to be close to high spin; this would lead to a value of $\mu_{eff}(U^{4+})$ on the smaller side compared with those observed in many U^{4+} compounds [40].

Regarding the other fitting parameters, the positive Weiss temperature implies that the main magnetic coupling is ferromagnetic and the temperature independent term (χ_0) is close to the core electron diamagnetism [41].

Fig. 8 shows the magnetization M vs. field H at 5 K and 298 K. At 298 K M increases linearly with T because of the paramagnetic nature of the magnetic state. However, the 5 K data show hysteresis, and the magnetization plateau occurs above 20 kOe with a magnetization moment of about 6 μ_B/f.u. Note that there are small changes in slope at about −400 Oe and +400 Oe (Fig. 8b) that may be related to the metamagnetic phase transition. The magnetization at the plateau is very much smaller than possible combinations of the theoretical saturation magnetization moment ($M_{sat} = gJ\mu_B$) of free ions of U^{4+} (J = 4, g= 0.8) and Cr^{2+} ($J = S$ = 2, g = 2 for high-spin; $J = S$ = 1, g = 2 for low spin). For example, the total theoretical M_{sat} is 27.2 μ_B/f.u for high-spin Cr^{2+} and 23.2 μ_B/f.u for low-spin Cr^{2+}. Even for the unlikely case of non-magnetic Cr^{2+}, the theoretical value of M_{sat} (17.2 μ_B/f.u) is still larger than the observed magnetization at the plateau. It is obvious that the magnetic ions, especially U^{4+}, behave far from free ions because of the CEF effect or itinerant magnetism. It is also possible that the magnetization plateau originates from ferrimagnetism, where the net moment of one ferromagnetic sub-lattice is opposite to the other ferromagnetic sub-lattice. On the assumption of free magnetic ions, the

total magnetization at the plateau is the difference between the two saturation magnetization moments, which ranges between 11.2 and 15.2 μ_B/f.u. The magnetization still increases above the magnetization plateau, which may be an indication of ferrimagnetism. In this case, at much higher fields, another magnetization plateau with full saturation moment should occur. Note that in previous studies $Ir_2U_6S_{15.5}$, $Ir_2U_6Se_{15.5}$, and $Rh_2U_6Se_{15.5}$ were found to be antiferromagnetic [24].

4. Conclusions

The compounds $Rh_2U_6S_{15}$, $Cs_2Ti_2U_6Se_{15}$, $Cs_2Cr_2U_6Se_{15}$, and $Cs_2Ti_2U_6Te_{15}$ have been synthesized at 1173 K. All crystallize in space group O_h^9–*Im3m* of the cubic system with four formula units in the unit cell. $Rh_2U_6S_{15}$ has a framework structure that has three-dimensional channels. The compounds $Cs_2Ti_2U_6Se_{15}$, $Cs_2Cr_2U_6Se_{15}$, and $Cs_2Ti_2U_6Te_{15}$ have structures similar to that of $Rh_2U_6S_{15}$, but with Cs cations variably filling the channels. In one sample of $Cs_2Ti_2U_6Se_{15}$ and in $Cs_2Ti_2U_6Te_{15}$ the channels are filled, but in a second sample of $Cs_2Ti_2U_6Se_{15}$ and in $Cs_2Cr_2U_6Se_{15}$ the channels are partially filled. In all four structures the transition element is octahedrally coordinated by chalcogens and the uranium atom is coordinated by eight chalcogens in a bicapped trigonal-prismatic arrangement.

The magnetic susceptibility of $Cs_2Cr_2U_6Se_{15}$ above 100 K shows Curie-Weiss behavior with μ_{eff} = 8.0 μ_B, a value that can be explained better with both Cr and U magnetic contributions. The Weiss temperature of 51 K indicates ferromagnetic coupling between magnetic ions. The magnetic susceptibility increases very sharply around 84 K and is strongly dependent on whether the sample is field cooled or zero-field cooled. Such bifurcation and the temperature dependence are consistent with either a ferromagnetic or ferrimagnetic ground state.

Acknowledgments

Use was made of the IMSERC X-ray Facility at Northwestern University, supported by the International Institute of Nanotechnology (IIN). A portion of this work was performed at the National High Magnetic Field Laboratory, which is supported by NSF Cooperative Agreement No. DMR–1157490 by the State of Florida and by the DOE.

Supporting information

Crystallographic data in cif format for $Rh_2U_6S_{15}$, $Cs_2Ti_2U_6Se_{15}$-1, $Cs_2Ti_2U_6Se_{15}$-2, $Cs_2Cr_2U_6Se_{15}$ and $Cs_2Ti_2U_6Te_{15}$ have been deposited with FIZ Karlsruhe as CSD numbers 429178, 429179, 429180, 429181, and 429182, respectively. These data may be obtained free of charge by contacting FIZ Karlsruhe at +497247808666 (fax) or crysdata@fiz-karlsruhe.de (email).

References

[1] E. Manos, M.G. Kanatzidis, J.A. Ibers, Actinide Chalcogenide Compounds, in: L.R. Morss, N.M. Edelstein, J. Fuger (Eds.), The Chemistry of the Actinide and Transactinide Elements, 4th ed., Vol. 6, Springer, Dordrecht, The Netherlands, 2010, p. 4005-4078.

[2] D.E. Bugaris, J.A. Ibers, Dalton Trans. 39 (2010) 5949-5964.

[3] A.A. Narducci, J.A. Ibers, Chem. Mater. 10 (1998) 2811-2823.

[4] L.A. Koscielski, J.A. Ibers, Z. Anorg. Allg. Chem. 638 (2012) 2585-2593.

[5] N.K. Sato, N. Aso, K. Miyake, R. Shiina, P. Thalmeier, G. Varelogiannis, C. Geibel, F. Steglich, P. Fulde, T. Komatsubara, Nature (London) 410 (2001) 340-343.

[6] R.E. Baumbach, J.J. Hamlin, M. Janoschek, I.K. Lum, M.B. Maple, J. Phys.: Condens. Matter 23 (2011) 1-5.

[7] M.B. Maple, Physica C 341-348 (2000) 47-52.

[8] J.D. Thompson, E.A. Ekimov, V.A. Sidorov, E.D. Bauer, L.A. Morales, F. Wastin, J.L. Sarrao, J. Phys. Chem. Solids 67 (2006) 557-561.

[9] V. Mougel, L. Chatelain, J. Pécaut, R. Caciuffo, E. Colineau, J.-C. Griveau, M. Mazzanti, Nat. Chem. 4 (2012) 1011-1017.

[10] H. Noël, J. Padiou, J. Prigent, C. R. Seances Acad. Sci., Ser. C 272 (1971) 206-208.

[11] H. Noël, C. R. Seances Acad. Sci., Ser. C 277 (1973) 463-464.

[12] H. Noël, C. R. Seances Acad. Sci., Ser. C 279 (1974) 513-515.

[13] H. Noël, M. Potel, J. Padiou, Acta Crystallogr. Sect. B: Struct. Crystallogr. Cryst. Chem. 31 (1975) 2634-2637.

[14] H. Kohlmann, K. Stöwe, H.P. Beck, Z. Anorg. Allg. Chem. 623 (1997) 897-900.

[15] G.N. Oh, J.A. Ibers, Acta Cryst. E67 (2011) i46.

[16] T. Vovan, N. Rodier, C. R. Seances Acad. Sci., Ser. C 289 (1979) 17-20.

[17] H. Noel, R. Troc, J. Solid State Chem. 27 (1979) 123-135.

[18] M.D. Ward, A. Mesbah, S.G. Minasian, D.K. Shuh, T. Tyliszczak, M. Lee, E.S. Choi, S. Lebègue, J.A. Ibers, Inorg. Chem. 53 (2014) 6920-6927.

[19] I. Ijjaali, K. Mitchell, F.Q. Huang, J.A. Ibers, J. Solid State Chem. 177 (2004) 257-261.

[20] G.B. Jin, E. Ringe, G.J. Long, F. Grandjean, M.T. Sougrati, E.S. Choi, D.M. Wells, M. Balasubramanian, J.A. Ibers, Inorg. Chem. 49 (2010) 10455-10467.

[21] H. Noël, J. Padiou, J. Prigent, C. R. Seances Acad. Sci., Ser. C 280 (1975) 123-126.

[22] J. Yao, D.M. Wells, G.H. Chan, H.-Y. Zeng, D.E. Ellis, R.P. Van Duyne, J.A. Ibers, Inorg. Chem. 47 (2008) 6873-6879.

[23] G.N. Oh, E.S. Choi, J.A. Ibers, Inorg. Chem. 51 (2012) 4224-4230.

[24] A. Daoudi, H. Noël, J. Alloys Compd. 233 (1996) 169-173.

[25] J.-Y. Kim, D.L. Gray, J.A. Ibers, Acta Cryst. Sect. E: Struct. Rep. Online E62 (2006) i124-i125.

[26] A. Daoudi, H. Noël, Inorg. Chim. Acta 140 (1987) 93-95.

[27] A. Daoudi, H. Noël, J. Less-Common Met. 153 (1989) 293-298.

[28] G.N. Oh, E.S. Choi, J. Lu, L.A. Koscielski, M.D. Ward, D.E. Ellis, J.A. Ibers, Inorg. Chem. 51 (2012) 8873-8881.

[29] A. Daoudi, M. Potel, H. Noël, J. Alloys Compd. 232 (1996) 180-185.

[30] A. Mesbah, C.D. Malliakas, S. Lebègue, A.A. Sarjeant, W. Stojko, L.A. Koscielski, J.A. Ibers, Inorg. Chem. 53 (2014) 2899-2903.

[31] A. Mesbah, W. Stojko, S. Lebègue, C.D. Malliakas, L. Frazer, J.A. Ibers, J. Solid State Chem. 221 (2015) 398-404.

[32] A.J.K. Haneveld, F. Jellinek, J. Less-Common Met. 18 (1969) 123-129.

[33] M.D. Ward, A. Mesbah, M. Lee, C.D. Malliakas, E.S. Choi, J.A. Ibers, Inorg. Chem. 53 (2014) 7909-7915.

[34] Bruker APEX2 Version 2009.5-1 Data Collection and Processing Software,, Bruker Analytical X-Ray Instruments, Inc., Madison, WI, USA, 2009.

[35] G.M. Sheldrick, SADABS, 2008. Department of Structural Chemistry, University of Göttingen, Göttingen, Germany

[36] G.M. Sheldrick, Acta Crystallogr. Sect. A: Found. Crystallogr. 64 (2008) 112-122.

[37] L.M. Gelato, E. Parthé, J. Appl. Crystallogr. 20 (1987) 139-143.

[38] D. Palmer, CrystalMaker Software Version 2.7.7, 2013. CrystalMaker Software Ltd., Oxford, England

[39] P.A. Joy, P.S. Anil Kumar, S.K. Date, J. Phys.: Condens. Matter 10 (1998) 11049-11054.

[40] V. Sechovsky, L. Havela, Magnetism of Ternary Intermetallic Compounds of Uranium, in: K.H.J. Buschow (Ed.), Handbook of Magnetic Materials, 1st ed., Vol. 11, Elsevier,

Amsterdam, 1998, p. 1-290.

[41] E.A. Boudreaux, L.N. Mulay, Theory and Applications of Molecular Paramagnetism, Wiley International, New York, 1976.

Table 1. Crystallographic data for $Rh_2U_6S_{15}$, $Cs_2Ti_2U_6Se_{15}$-1, $Cs_2Ti_2U_6Se_{15}$-2, $Cs_2Cr_2U_6Se_{15}$, and $Cs_2Ti_2U_6Te_{15}$[a]

Compound	$Rh_2U_6S_{15}$	$Cs_2Ti_2U_6Se_{15}$-1	$Cs_2Ti_2U_6Se_{15}$-2	$Cs_2Cr_2U_6Se_{15}$	$Cs_2Ti_2U_6Te_{15}$
Crystal System	Cubic	Cubic	Cubic	Cubic	Cubic
$a = b = c$ (Å)	13.1990(9)	14.0029(4)	13.9062(8)	13.91840(3)	15.0130(4)
V (Å^3)	2299.4(5)	2745.7(2)	2689.2(5)	2696.30(17)	3383.8(3)
$R(F)$[b]	0.0247	0.0178	0.0212	0.0196	0.0340
$R_w(F_o^2)$[c]	0.0973	0.0524	0.0668	0.0397	0.0855
q[d]	0.0436	0.0157	0.0169	0.0080	0.0000

[a]For all compounds T = 100 K, Z = 4, space group = O_h^9–$Im\bar{3}m$

[b]$R(F) = \Sigma \big| |F_o| - |F_c| \big| / \Sigma |F_o|$ for $F_o^2 > 2\sigma(F_o^2)$. [c]$R_w(F_o^2) = \{\sum [w(F_o^2 - F_c^2)^2] / \sum wF_o^4\}^{½}$ for all data. [d]$w^{-1} = \sigma^2(F_o^2) + (qF_o^2)^2$ for $F_o^2 \geq 0$; $w^{-1} = \sigma^2(F_o^2)$ for $F_o^2 < 0$.

Table 2. Selected interatomic distances for $Rh_2U_6S_{15}$[a]

$Rh_2U_6S_{15}$	Distance | (Å)
U1−S2 × 2	2.754(1)
U1−S1 × 4	2.796(1)
U1−S1 × 2	2.856(2)
U1−Rh1 × 2	3.412(1)
U1−U1 × 4	3.991(1)
Rh1−S1 × 6	2.382(2)
Rh1−U1 × 6	3.412(1)

[a]All interatomic distances have been rounded.

Table 3. Selected interatomic distances for $Cs_2M_2U_6Q_{15}$ (M = Ti, Cr, *Q* = Se, Te) (Å) [a]

	$Cs_2Ti_2U_6Se_{15}$-1	$Cs_2Ti_2U_6Se_{15}$-2	$Cs_2Cr_2U_6Se_{15}$	$Cs_2Ti_2U_6Te_{15}$
U1−*Q*1 × 4	2.942(1)	2.926(1)	2.924(1)	3.170(1)
U1−*Q*2 × 2	2.956(1)	2.932(1)	2.933(1)	3.156(1)
U1−*Q*1 × 2	3.042(1)	3.020(1)	3.032(1)	3.264(1)
U1−*Q*1 × 2	3.605(1)	3.581(1)	3.585(1)	3.870(1)
U1−U1 × 4	4.268(1)	4.235(1)	4.237(1)	4.563(1)
U1−Cs1	4.092(1)	4.057(1)	4.057(1)	4.363(1)
U1−Cs2 × 2	4.695(4)	4.821(6)	4.867(7)	4.988(1)
U1−Cs1 × 2	5.025(1)	4.991(1)	4.996(1)	5.391(1)
*M*1−*Q*1 × 6	2.578(1)	2.566(1)	2.531(1)	2.787(1)
*M*1−U1 × 6	3.605(1)	3.581(1)	3.585(1)	3.870(1)
Cs1−*Q*2 × 4	3.501(1)	3.477(1)	3.480(1)	3.753(1)
Cs1−*Q*1 × 8	3.637(1)	3.606(1)	3.652(1)	3.883(1)
Cs2−*Q*1 × 4	3.596(6)	3.787(9)	3.839(10)	3.733(4)

[a]All interatomic distances have been rounded.

Figure Legends

Fig. 1. The framework structure of $Rh_2U_6S_{15}$.

Fig. 2. Coordination of Rh in the structure of $Rh_2U_6S_{15}$.

Fig. 3. Coordination of U in the structure of $Rh_2U_6S_{15}$.

Fig. 4. Framework structure of $Cs_2M_2U_6Q_{15}$ (M = Ti, Cr, Q = Se, Te) with Cs1 atoms in the channels.

Fig. 5. Framework structure of $Cs_2M_2U_6Q_{15}$ (M = Ti, Cr, Q = Se, Te) showing the positions of the Cs2 atoms in the channels.

Fig. 6. Temperature dependence of the magnetic susceptibility for $Cs_2Cr_2U_6Se_{15}$.

Fig. 7. The inverse magnetic susceptibility vs. temperature for $Cs_2Cr_2U_6Se_{15}$.

Fig. 8. Magnetization data for $Cs_2Cr_2U_6Se_{15}$ at 298 K and 5 K.

Figure 1

Click here to download high resolution image

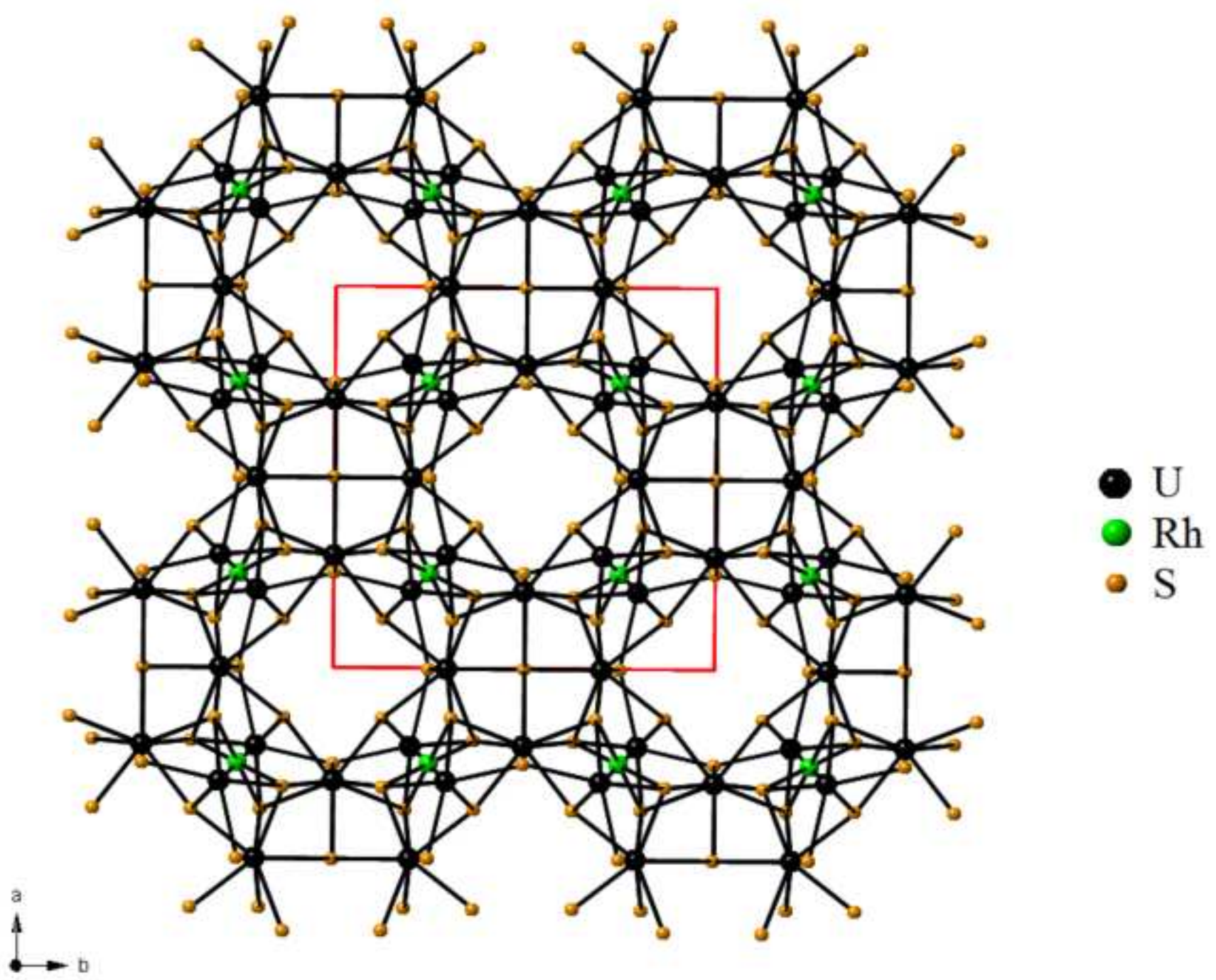

Figure 2

Click here to download high resolution image

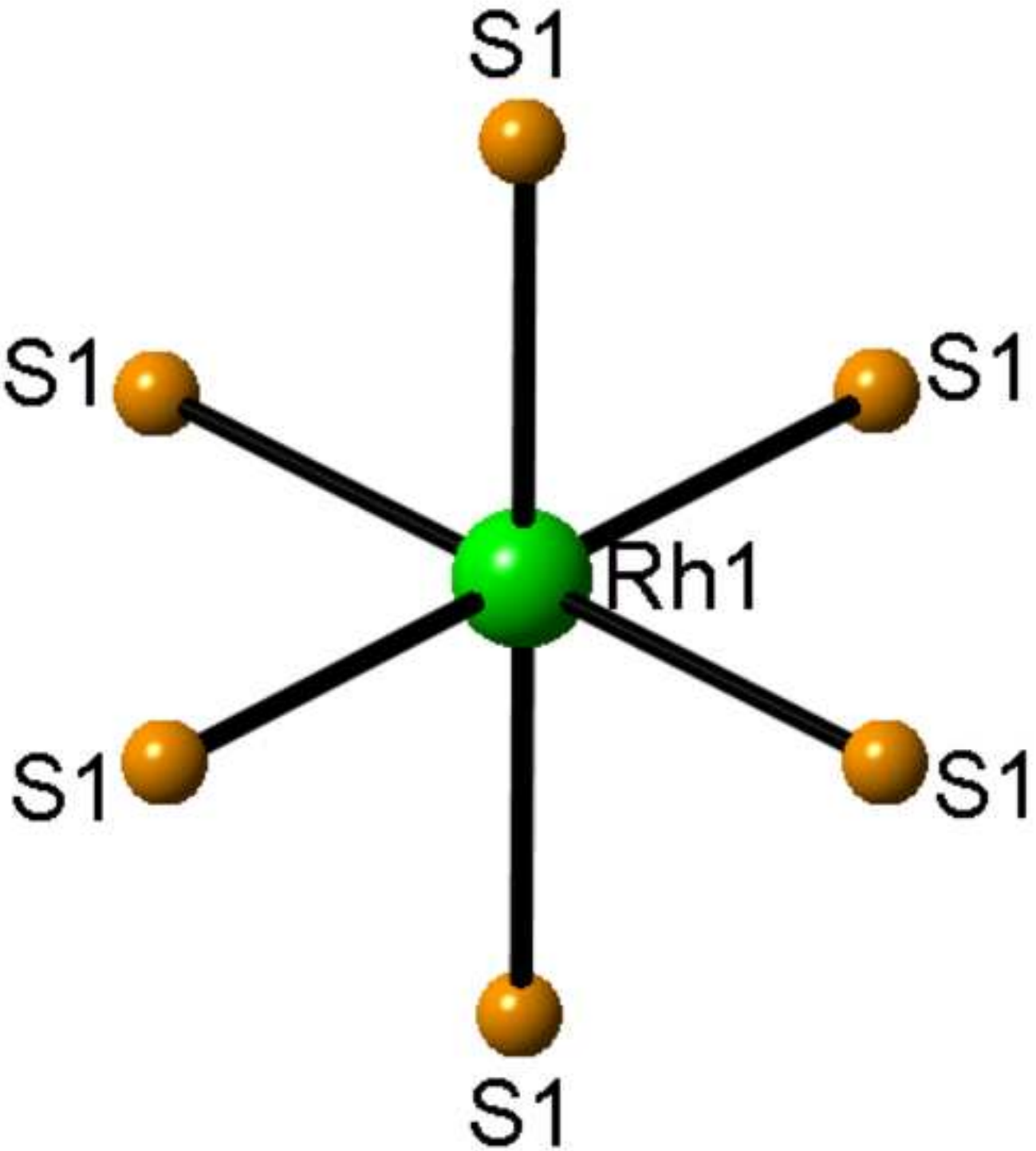

Figure 3

Click here to download high resolution image

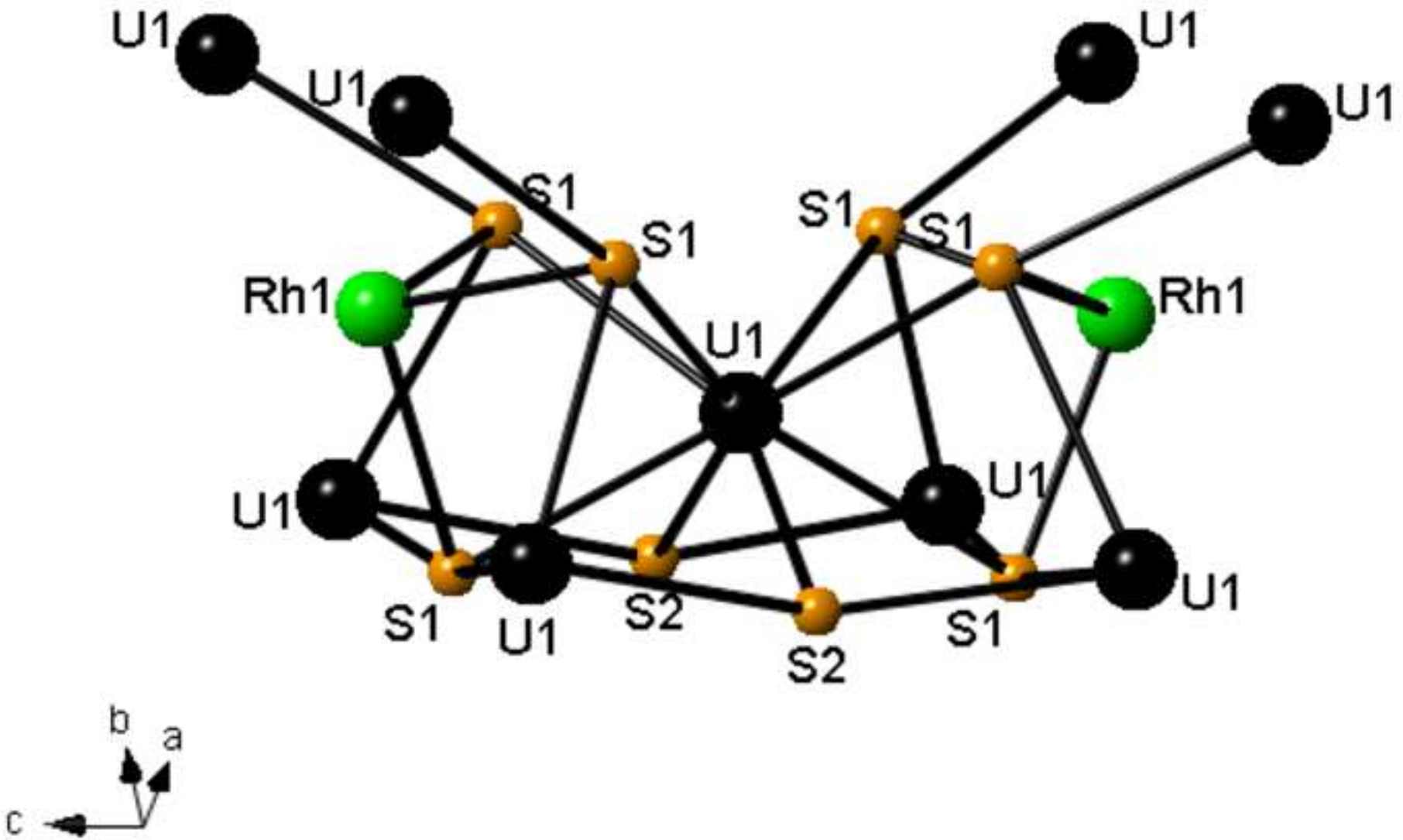

Figure 4

Click here to download high resolution image

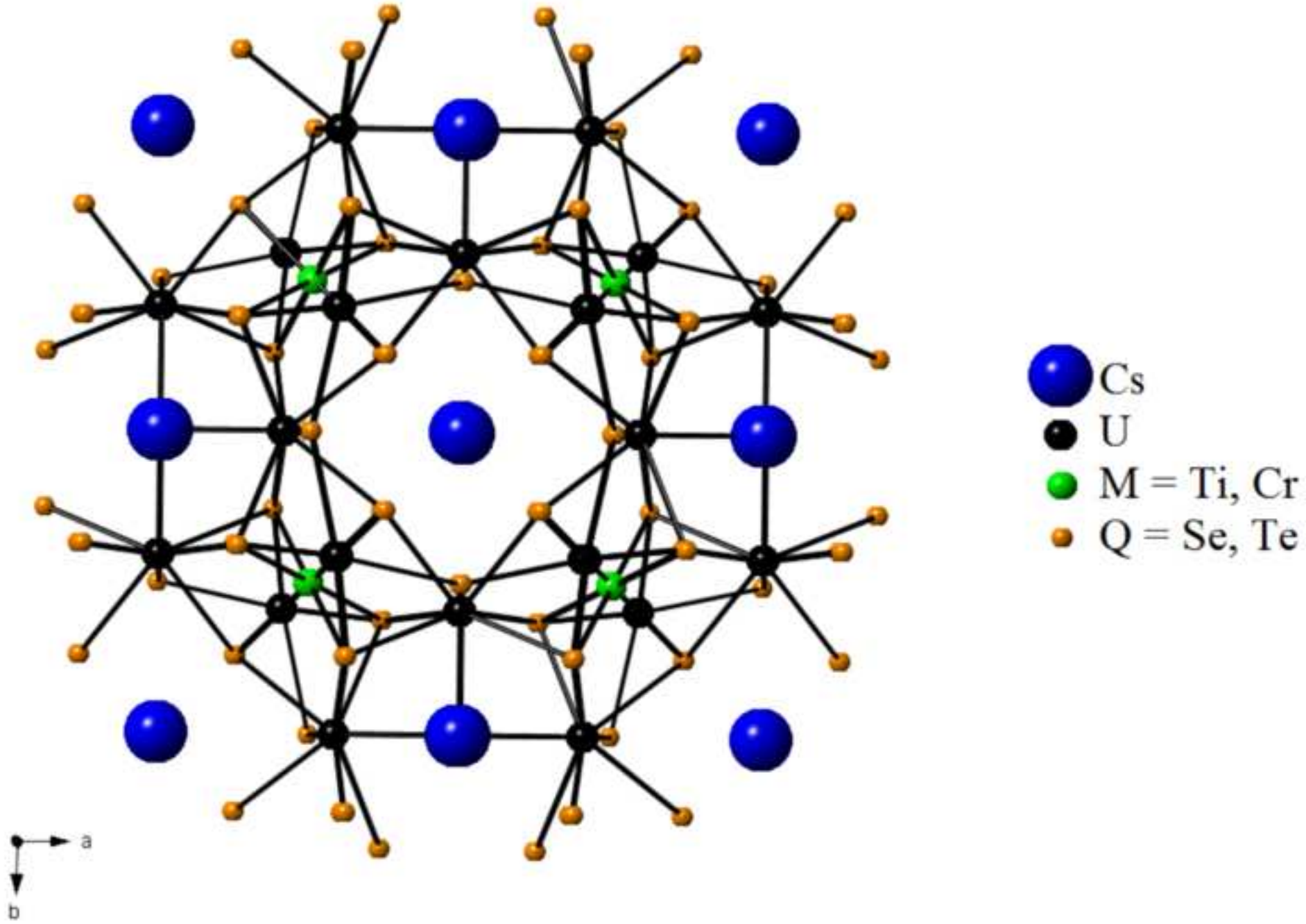

Figure 5

Click here to download high resolution image

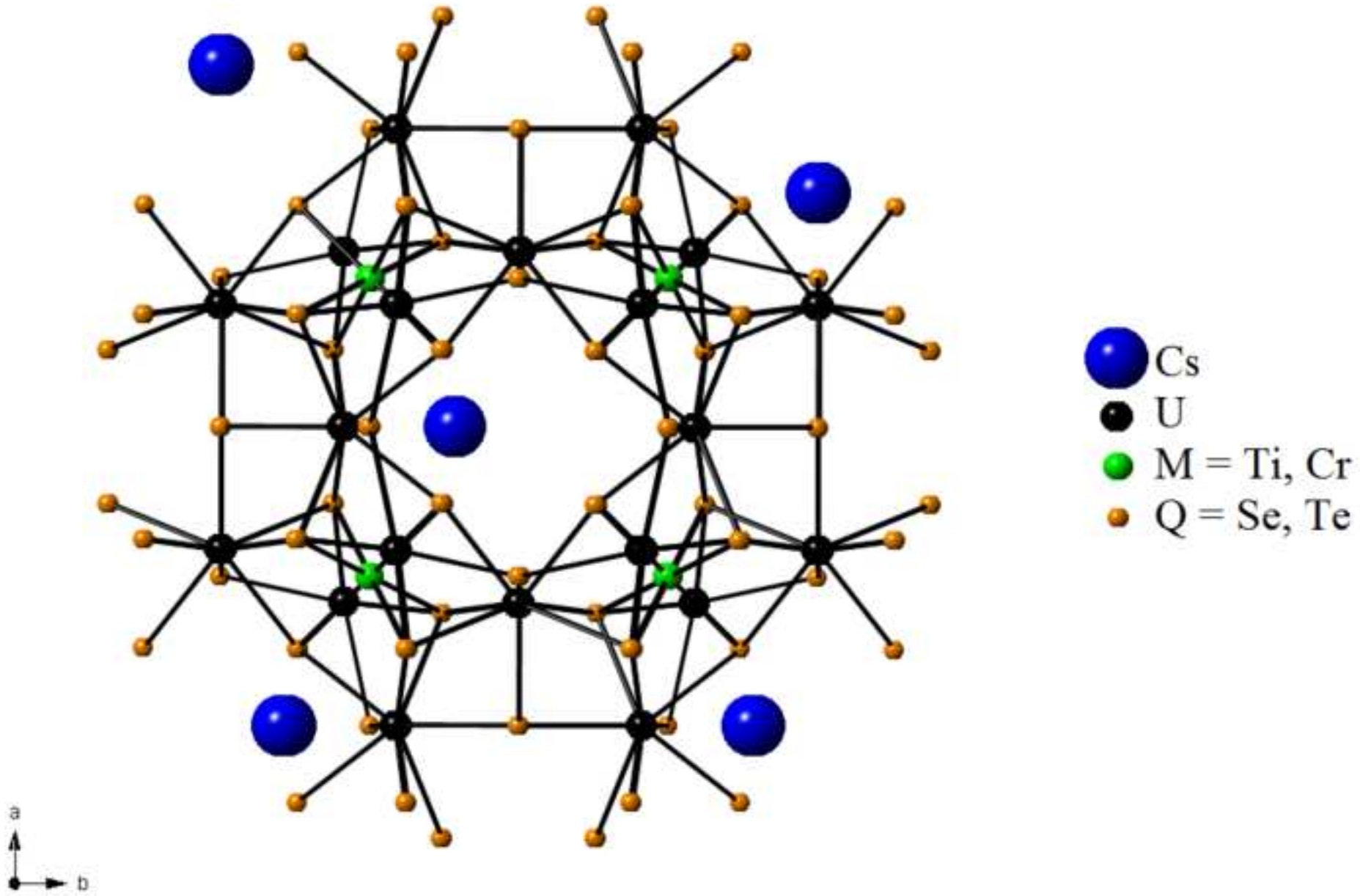

Figure 6

Click here to download high resolution image

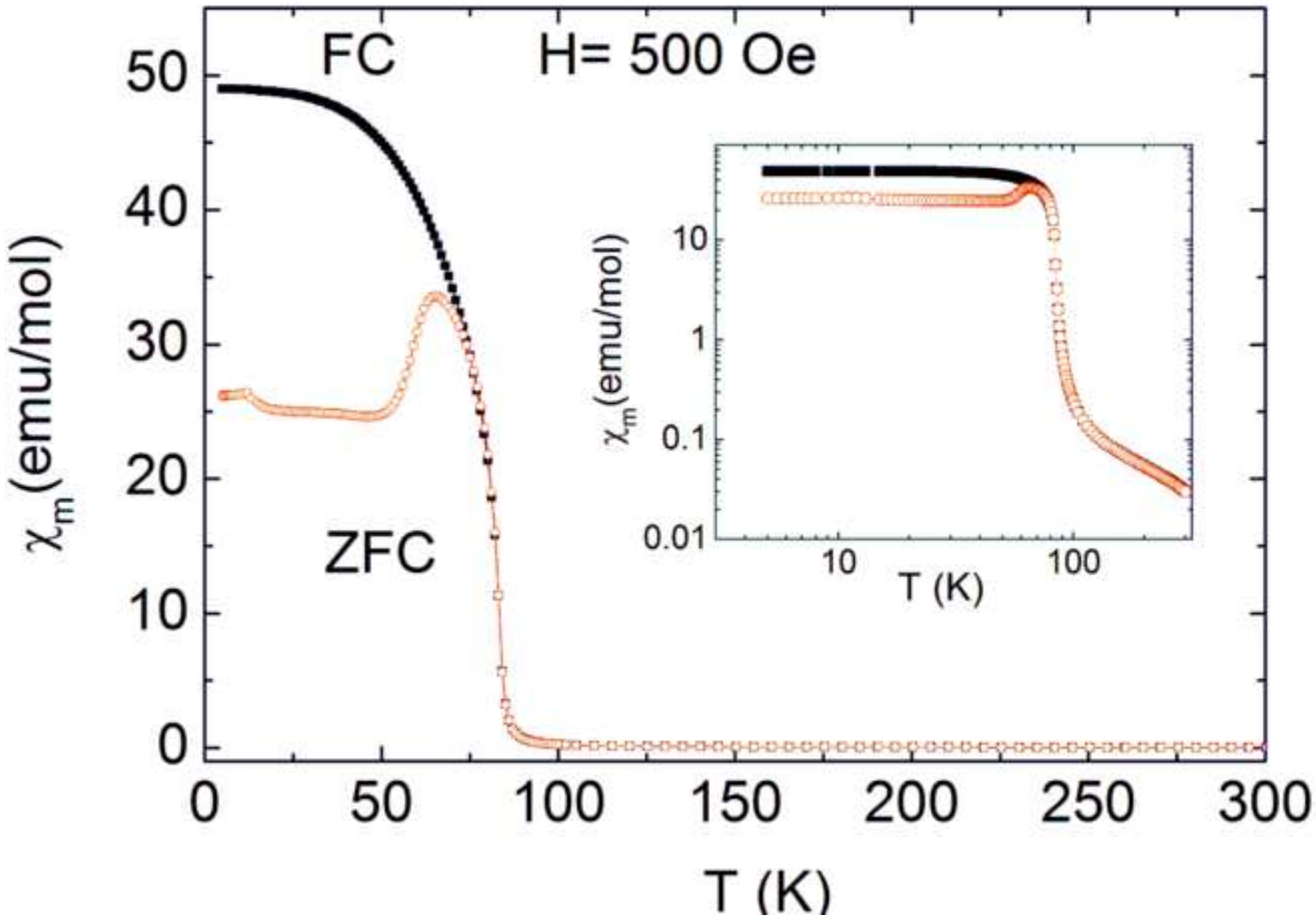

Figure 7

Click here to download high resolution image

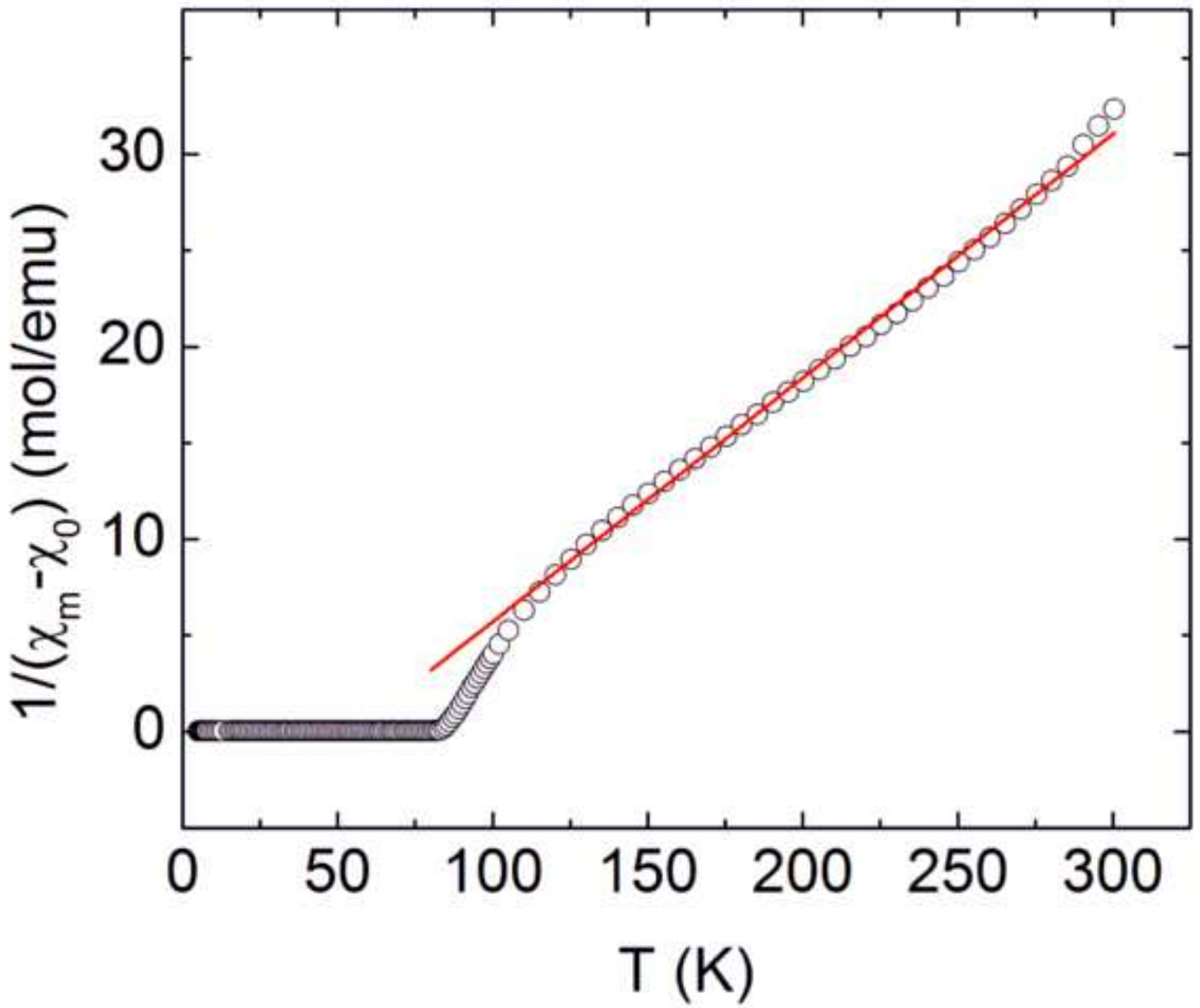

Figure 8

Click here to download high resolution image

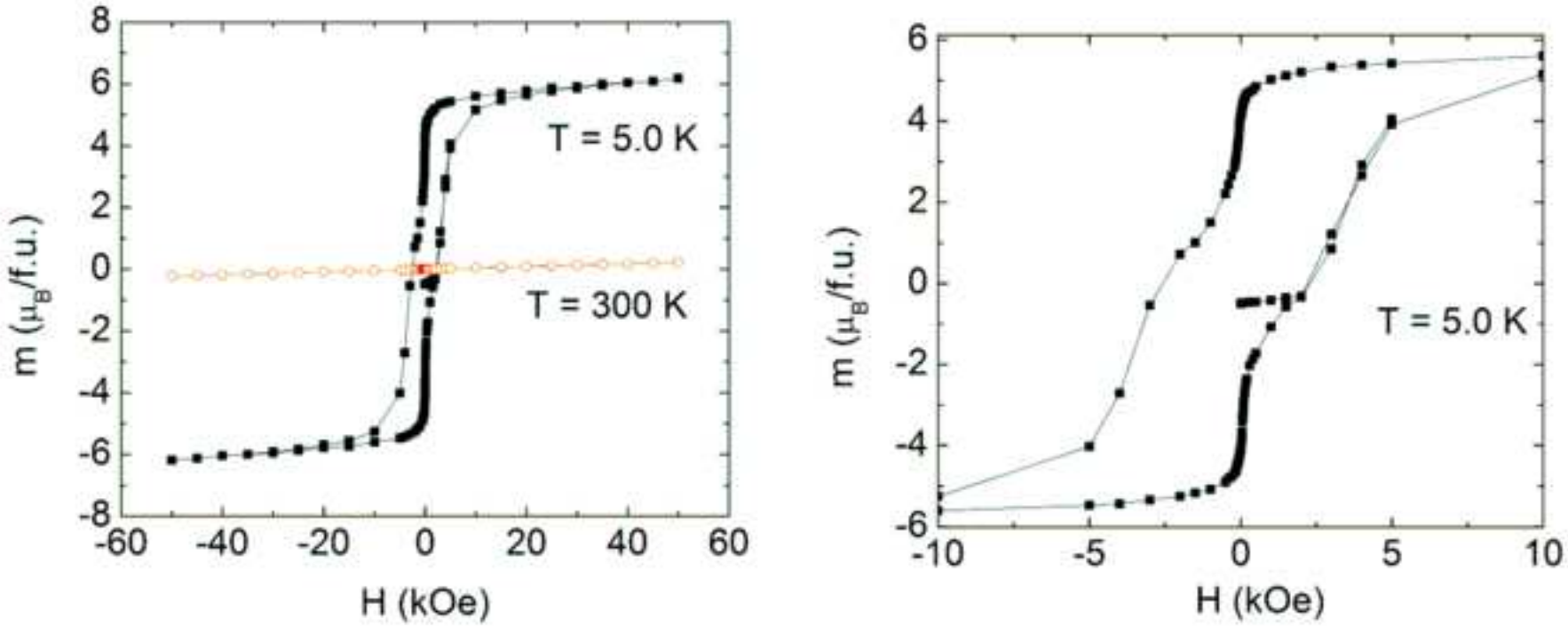

Graphical Abstract (TOC Figure)
Click here to download high resolution image